Available online at www.sciencedirect.com

ScienceDirect

Proceedings of the Combustion Institute 35 (2015) 3565–3572

Proceedings of the Combustion Institute

www.elsevier.com/locate/proci

Experimental investigation of structure and stabilization of spray oxyfuel flames diluted by carbon dioxide

G. Cléon, D. Honoré, C. Lacour, A. Cessou *

CORIA – CNRS UMR6614, University & INSA of Rouen, F-76801 St Etienne du Rouvray, France

Available online 30 June 2014

Abstract

Oxycombustion diluted by recirculating flue gases is one of the most advanced innovating combustion technique to adapt carbon capture and storage (CCS) to industrial combustion plants. The dilution by flue gases with a large amount of CO_2 impacts the flame behavior in terms of combustion efficiency, pollutant emission, radiative transfer and flame stabilization. The present paper investigates, at lab-scale, the effect of CO_2 dilution on a spray oxyfuel flame in terms of flame structure and stabilization. A burner is well designed such that the boundary conditions may be accurately measured and be suitable to provide a confident database. A central spray of ethanol is surrounded by a O_2–CO_2 coflow. The coflow is modular to investigate the effect of CO_2 content separately from the coflow velocity. Size-classified Phase Doppler Anemometry characterizes the spatial non-homogeneity in size and velocity. The average flame structures are observed by OH^* chemiluminescence and complementary instantaneous flame observations by OH Planar Laser Induced Fluorescence. Three types of flames are observed with a trailing flame exhibiting a double structure specific to two-phase combustion and linked to the competition between vaporization, chemical and mixing time scales. The amount of CO_2 in the oxidant affects strongly the flame structure and stabilization. It modifies drastically the chemical time, the flame temperature, and thus the vaporization time and the size dispersion. The outer flame of the double structure is always diffusion-like while the inner flame changes from diffusion-like to premixed-like when the vaporization time shortens. This investigation shows the additional effects of CO_2 dilution on spray combustion.

Keywords: Oxyfuel combustion; Spray combustion; CO_2; Lift-off

1. Introduction

Oxycombustion diluted by recirculating flue gases is one of the most advanced innovating combustion technique to adapt carbon capture and storage (CCS) to industrial combustion plants [1,2]. High efficiency of the CCS process behind

* Corresponding author. Address: CORIA – CNRS UMR6614, Université de Rouen, F-76801 St Etienne du Rouvray, France. Fax: +33 (0)2 32 91 85 04.

E-mail address: armelle.cessou@coria.fr (A. Cessou).

http://dx.doi.org/10.1016/j.proci.2014.06.028

the combustion chamber requires a large amount of CO_2 in flue gas, which is ensured by reinjection of CO_2 extracted from the stack, in the burner to dilute fuel and oxygen reactants. These specific operating conditions have strong effects on flame stability, heat transfer and pollutant emissions. Several experimental investigations already exist concerning different fuels, either coal [3,4] or gaseous fuels [5–7]. With propane, Andersson et al. [5] have compared combustion in air and O_2/CO_2 atmosphere. Significant difference is observed for flame radiation intensity. Similar overall combustion behavior of air flame is obtained in O_2/CO_2 oxidant with higher oxygen concentration. Large concentrations of CO_2 in the oxidizer can also induce important CO emissions as observed by Amato et al. [6] in a swirl flame and Heil et al. [7] in a flameless combustion facility.

The present experimental study focuses on the effect of CO_2 content on the structure and stabilization of spray oxyfuel flames. A simplified configuration with well-defined inlet and boundary conditions is chosen to provide data suitable for the building of a database. It consists in a two-phase flow of a well-known pure substance with simple and well-controlled aerodynamic conditions. A central spray with size distribution independent of the gas flow velocity is surrounded by a modular O_2–CO_2 coflow to investigate the effect of CO_2 concentration separately from the influence of the coflow velocity Ethanol is chosen as fuel for its well-known thermodynamics data and chemical kinetics model. The choice of this pure liquid fuel is driven by the wish to focus the study on the impact of two-phase transport and evaporation on diluted oxyfuel combustion features in a relative simple configuration in terms of vaporization and chemistry, and to provide confident data for development and validation of numerical modeling, that will be used then for simulations of industrial applications with more complex configurations and liquid fuel.

The spray dispersion and aerodynamics are investigated by Phase Doppler Anemometry (PDA) and Laser Doppler Velocimetry (LDV). The flame structures are observed by OH^* chemiluminescence and OH Planar Laser Induced Fluorescence (PLIF), showing a main trailing flame with a double structure specific to two-phase combustion [8–12]. The change in the CO_2 content modifies drastically the chemical time, the flame temperature, and will modifies locally the vaporization time and the droplet size distribution, leading the flame to be partially premixed [11]. The outer flame of the double structure is always diffusion-like while the inner flame changes from diffusion-like to premixed-like when the vaporization time shortens.

2. Experimental set-up

A coaxial burner composed of a pressure injector fed by ethanol and surrounded by CO_2–O_2 coflow is located at the bottom of a combustion chamber of 1 meter long and 400 mm inner diameter with a water-cooled double stainless-steel casing equipped with large windows. For all the operating conditions, the thermal power is 23.3 kW and the global equivalence ratio is $\phi = 0.975$. A modular burner is designed to offer well-defined aerodynamics inlet conditions suitable for building of a database. The CO_2–O_2 mixture is controlled by mass flow controllers, and several coflow velocities are obtained for the same CO_2 content by changing the coflow diameter, D_{co} (Fig. 1). The dilution ratio, α, is defined as the volume fraction of CO_2 in the oxidant mixture. The liquid injector is a simplex injector (Delavan WDB0.75-30) with a 30° cone angle and a nozzle orifice of 230 μm diameter. The resulting spray consists in a conical liquid sheet, which breaks up at 6 mm from the nozzle as observed from photography of the spray, Mie scattering imaging or very low level of PDA validation below this height. In our experimental configuration, the use a pressure injector surrounded with coflow of moderate velocity makes this break-up length independent from the coflow velocity.

Mean flame structures are obtained from OH^* chemiluminescence imaging by using an UV CCD camera (Photometrics, CoolSnap) with a UG11 filter (Schott). The mean tomographic representation of the flame structure is worked out by Abel's inversion based on the axisymmetry of the configuration and that the convergence of the average image obtained by the high number of individual images (100) and the exposure time ranging between 15 and 100 ms depending on the flame stability and luminosity.

Characterization of the spray is determined by a PDPA system (Dantec) with back-scattering and 30°-front-scattering probes. The measurement volume is 150 μm × 150 μm × 3.5 mm. At each

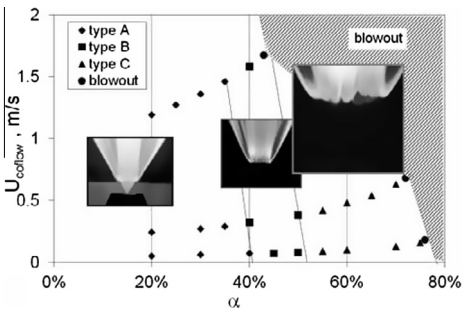

Fig. 1. Stability diagram.

measurement location, 20,000 data are sampled for a maximum time of 90 s, allowing statistical size-classified study of droplet velocity [8,13]. Because of the geometry of the spray, the measurements are only possible beyond 6 mm. The minimum number of data is 4000 noticed when the time of 90 s is reached. These small values are only observed at the tip of the liquid sheet and in the very dilute region of the spray on the axis far away from the nozzle. Beside the spray, fresh gas velocity of the co-flow is determined by LDV in back-scattering configuration by seeding the coflow by di-ethyl-hexyl-sebacate droplets with diameters less than 5 μm. At each measurement location, 10,000 data are recorded in coincidence mode or the acquisition is ended after a maximum of 60 s.

Instantaneous 2D images of the oxyfuel flame structures are obtained by OH PLIF. An intensified CCD camera (PIMAX) equipped with a UV lens (f/2.8) is synchronized with a tunable dye laser pumped by a Nd-YAG laser (Quantel) shaped in a vertical laser sheet (6 cm high) crossing the flame through a symmetry plane. The laser wavelength (282.67 nm) is spectrally tuned on the $Q_1(5)$ line of the ($A^2\Sigma$, $v' = 1 - X^2\Pi$, $v'' = 0$) band of OH. A set of spectral filters (1xUG11 and 2xWG280) is used to reject the Mie scattering of particles and then collect only OH fluorescence. For few experiments, the laser wavelength is detuned from the OH absorption line and one WG280 filter is removed to collect instantaneous images of Mie scattering of droplets alone.

OH Planar Laser Induced Fluorescence (PLIF) is a qualitative marker of the combustion regime. It is known to be a marker of burnt gases and diffusion and premixed flames can often be distinguished from the gradient and the thickness of the OH zone [14]. In diffusion flames, the OH signal is maximal around stoichiometry and decreases on either side with a thickness linked to the diffusion process. In a premixed flame, OH is present in all the burnt gases at high temperature and it is a good marker of the interface of fresh/burnt gases by the high signal gradient [14]. This simplified description can obviously be affected in turbulent flows. In the following, where the purpose is to qualitatively describe the change in flame properties according to the CO_2 content of the coflow, we will identify schematically the diffusion reaction zones as fine and symmetric OH zones and the premixed flame fronts as non-symmetric zones with a sharp gradient on one side, and a very low on the other side.

3. Results and discussion

3.1. Stability diagram

Three flame structures are observed depending on coflow velocity and α dilution ratio (Fig. 1). The first flame type, labeled A, is observed for low values of α. This flame is anchored at the nozzle by a small conical central flame. A main trailing flame stabilizes outwardly at the tip of the liquid sheet. When α increases, the conical central flame extinguishes and only the main trailing flame remains, still anchored at the extremity of the liquid sheet (type B). For higher dilution ratios (α >50%), the main trailing flame lifts off from the tip of the liquid sheet and stabilizes downstream (type C).

For α greater than 45%, flame blow-off is observed at $U_{bo} = 1.6$ m/s for $\alpha = 45\%$ and $U_{bo} = 0.7$ m/s for $\alpha = 65\%$. A dramatic decrease in the blow-out velocity is observed at $\alpha = 70\%$ with $U_{bo} = 0.15$ m/s and the flame is always extinguished for dilution ratio greater than 76% in our co-axial configuration at ambient temperature.

Figure 2 presents the lift-off height of the main trailing flame versus α for the three coflow diameters: the flame stabilization is mainly controlled by α and the 3 types of flames can be easily distinguished. For the type A (α <40%), the lift-off height is independent of α and the coflow velocity, since the flame is anchored at the tip of liquid sheet and the conical central flame exists. For the type B (40% < α < 50%), the lift-off height is moderate and varies from 5 mm to 7 mm independently of the coflow velocity. For the type C (α >50%), the flame is lifted off at a height increasing rapidly with α and almost independent of the coflow velocity. As in gas jet flames [15,16], a higher lift-off height could be expected when the coflow velocities increase. Here the spray affects the aerodynamics of the flow as illustrated in Fig. 3 presenting the gas velocity in the vicinity of the flame for two coflow velocities and $\alpha = 60\%$. The spray imposes an intense deflection of the coflow towards the centerline leading to very similar aerodynamic conditions at the flame base despite the two different exit velocities (0.51 m/s for $D_{co} = 95$ mm and 0.11 m/s for $D_{co} = 200$ mm). In the region of the flame stabil-

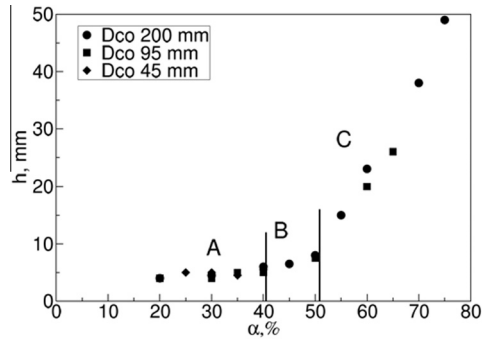

Fig. 2. Lift-off height of the trailing flame.

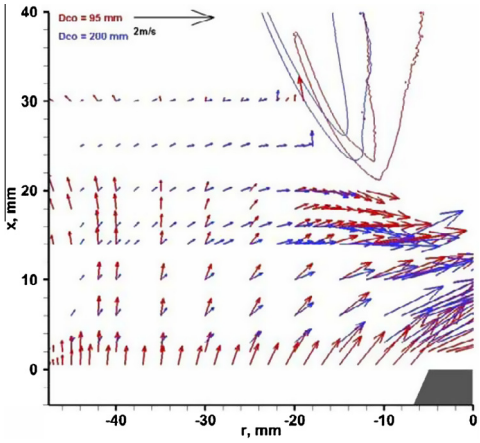

Fig. 3. Gas velocity field for $a = 60\%$ superimposed to the outlines of chemiluminescence, for $D_{co} = 95$ mm (red) and $D_{co} = 200$ mm (blue).

ization, the aerodynamics of the gas is controlled by the momentum of the spray and becomes almost independent of the coflow velocity.

3.2. Two-phase flow

In order to provide an overview of the size distribution of the spray, Table 1 gives two mean diameters for two characteristic positions: at the tip of the liquid sheet ($r = -4$ mm; $x = 6$ mm) and on the axis ($r = 0$ mm; $x = 6$ mm).

The measurements upstream the lifted flames (type C) can be used as representative data of the spray in cold condition. The mean diameters of types C at (−4; 6) shows the polydispersion of the spray with a distribution spreading from 15 μm to 90 μm, peak value around 40 μm, and Sauter mean diameter of 54 μm. At this location, the small droplets represent a minor part of the spray. The mean diameters of the two C-flames presented show that the size distributions are very similar for two coflow velocities confirming that the choice of a pressure nozzle makes the spray properties almost independent of the gas aerodynamics. The mean diameters at the centerline are clearly different from the data at the tip of the liquid sheet, showing the spatial in homogeneity of the spray. In its central part, the diameters are small and the spray is homogeneous in size.

When the flame anchors at the tip of the liquid sheet (types A and B), the mean diameters at (−4; 6) slightly increase, which is characteristic of the evaporation of the polydisperse sprays due to the disappearance of the smallest droplets. Due to the size homogeneity near the centerline, the evaporation has less impact on the mean diameters at (0; 6) what is consistent with the observations of Kourmatzis et al. [17].

For each type of flame, the coflow velocity has a very little impact on the spray properties (Table 1) and the aerodynamics is mainly controlled by the momentum of the spray (Fig. 3). Therefore in the following, the flow and flame properties will be described for $D_{co} = 95$ mm in diameter. The aerodynamics of the spray is analyzed by size classes. An illustration of this analysis is given on the velocity maps of 4 size classes superimposed on the Abel's inversion of OH^* emission (Fig. 4). For lifted flames (type C), the near-field maps are representative of the non-reacting spray. The outline of the spray is the same for the three flame types. The largest droplets (>50 μm) are ejected exclusively from the tip of the liquid sheet, with an angle of 35°. These large droplets have a ballistic behavior: they are ejected at the velocity of the liquid sheet (36 m/s) and they retain long this high velocity along a direction of 30°, leading to short residence time in the first stages of the flow. The droplets of intermediate size are mainly ejected with an angle of 30° with a maximum velocity of 36 m/s around $r = -3$ mm. While the smallest droplets are present through the complete section of the spray, they represent numerically the major part of the spray around the axis. At the tip of the liquid sheet, they are ejected with an angle of 30° and a velocity of 29 m/s. On the centerline, they move parallel to the axis with a slower velocity around 15 m/s. Due to their rapid evaporation, they are confined to the inner part of the flow, where they conserve this velocity. At all the locations investigated the small droplets do not follow the gas motion and keep high velocities. Moreover their velocity fluctuations are high due to the high velocity of ejection and the evaporation in

Table 1
Mean diameters at the tip of the liquid sheet and on the centerline at $x = 6$ mm.

			$r = -4$ mm, $x = 6$ mm		$r = 0$ mm, $x = 6$ mm	
α	D_{co}	Type	D_{10}	D_{32}	D_{10}	D_{32}
30%	45	A	46	65	9.5	13
30%	95	A	43	58	12	15.5
40%	45	B	45.5	67	10	14
40%	95	B	44	60	11	14
60%	95	C	41	54	8.5	13
60%	200	C	40	55	14	16

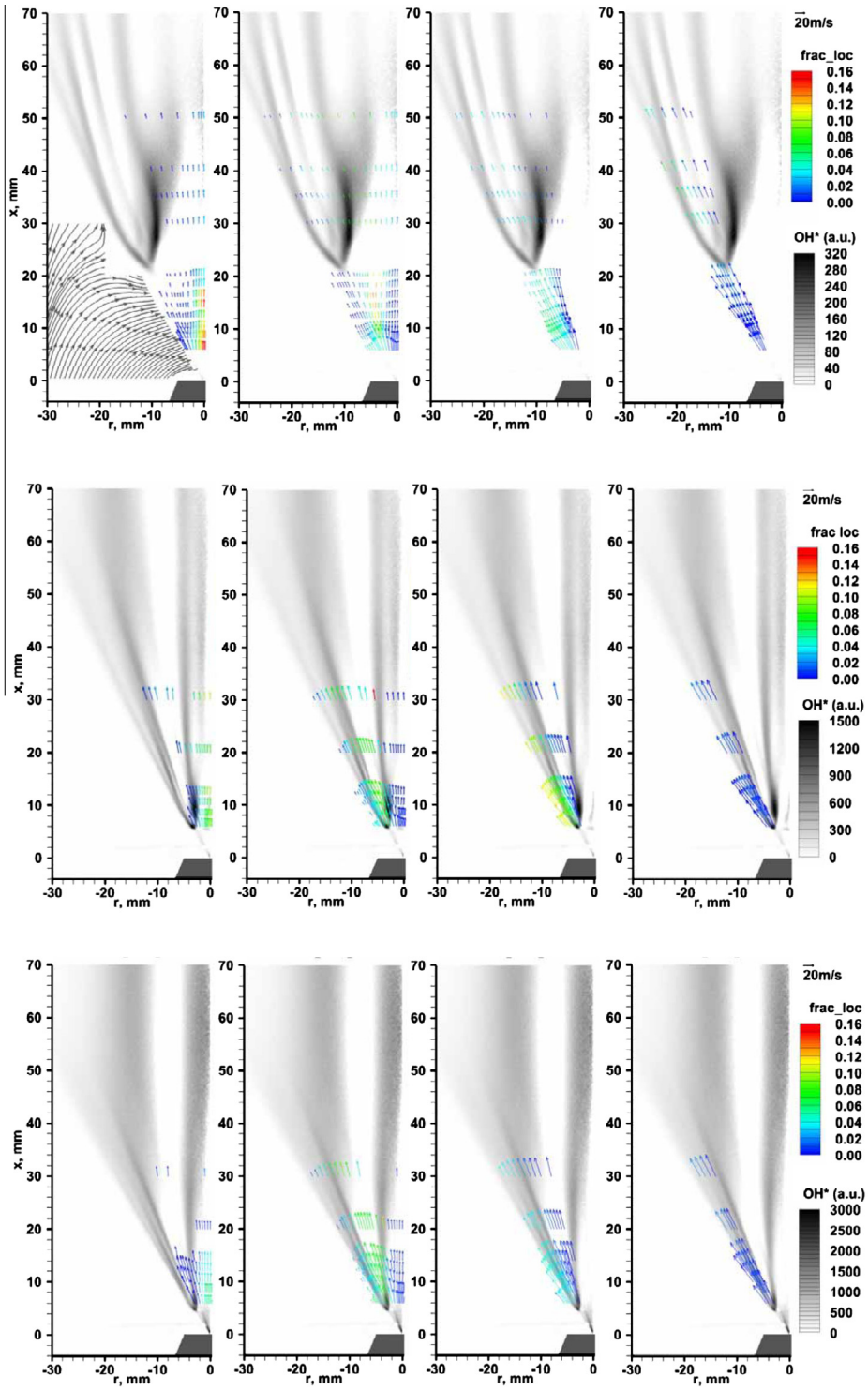

Fig. 4. Velocity vector plots of the droplet for 4 size classes (5, 25, 50, 100 μm from left to right) superposed on the average flame structure from Abel's inversion for $D_{co} = 95$ mm and three values of α, 60% for type C, 40% for type B and 30% for type A. The colormap indicates the local numerical fraction.

proximity of the flame, which leads the largest droplets to feed the smaller size class.

For type C, for which the flame is lifted downstream, the numerical fraction of the smallest droplets remains high around the axis. When the flame is stabilized close to the injector, especially for type A, the numerical fraction of the smallest droplets decreases dramatically showing the rapid evaporation of the smallest droplets.

3.3. Flame structures

The spray heterogeneity in size and velocity affects the flame structures. First, it can be denoted that the main trailing flame exhibits a double structure for the three flame types (Fig. 3), as observed by Marley et al. [10] in air combustion. OH PLIF and Mie scattering images are presented in Fig. 5 to illustrate the instantaneous flame structure and to analyze its combustion regimes. The largest droplets are ejected towards the double flame gap, where the proximity of the two flames leads to a rapid evaporation demonstrated by the narrowing of the diameter pdfs and their shift to smaller diameters: disappearance of the smallest droplets and a rapid size reduction of the largest droplets. The fuel vapor produced within the double-flame gap makes possible an outer flame with the oxidant coflow, which exhibits for the three types a diffusion-like feature with a fine symmetric profile of OH PLIF.

The structure of the inner reaction zone of the double trailing flame is strongly affected by α (Fig. 5), via the competition between the vaporization, chemical and mixing time scales. The burning velocity and the adiabatic flame temperature are worked out by the COSILAB software [18] with the kinetic mechanism proposed by Leplat et al. [19]. The vaporization rate is estimated from the d^2-law [20] in quasi-steady condition and by an iterative determination of the surface temperature of the droplets [11]. The ratio of the vaporization times at T_F and 300 K (Table 2) indicates qualitatively the impact of the presence of the flame on the vaporization rate.

For the high values of α (type C), the inner flame is connected to the outer one. In the first centimeters, it exhibits a diffusion-like feature before thickening. Some full and hollow pockets of OH are observed on the axis. They are representative of two-phase combustion [21] and depend on the local density of droplets (droplets size and inter-droplet distance) and the amount of oxidizer around them. They illustrate the complexity of the two-phase turbulent mixing in this region where the spray shows locally a large polydispersion (Fig. 3). The broadening of the OH profile and the presence of burning pockets show the more complex structure of the inner flame exhibiting a partially premixed regime [11]. The continuity of the flame structure at the bottom of the lifted flame without extinction, while the large droplets cross it, is linked to the low density of the droplets at this height due to the radial expansion of the flow.

Table 2
Flame properties and relative vaporization time.

α	S_L (m/s)	T_F (K)	S_{TF} (m/s)	τ_{vap} (300 K)/τ_{vap} (T_F)
60%	0.5	2415	1.4	117
40%	1.2	2693	3.6	137
30%	1.5	2791	4.6	144

For type B, the aspect of the inner flame is clearly modified. It shows that the inner part of the trailing flame is no more connected to the outer one due to the large amount of large droplets crossing the flame at the tip of the liquid sheet. The inner OH zone is thicker than for type C, with sharp gradient of OH PLIF signal along the inner droplet cloud. The dissymmetry of the radial OH profile illustrates the partially premixed structure of this inner flame. The higher concentration of O_2 leads to large changes in combustion time scale and flame temperature (Table 2), and subsequently in the vaporization rate given at T_F for indication. The central part of the spray is composed of small droplets with small polydispersion. Due to the higher concentration of O_2, the temperature of the inner flame is higher and leads to the rapid vaporization of the small droplets present in the central part as shown by the corrugated inner OH outline matching the boundary of the

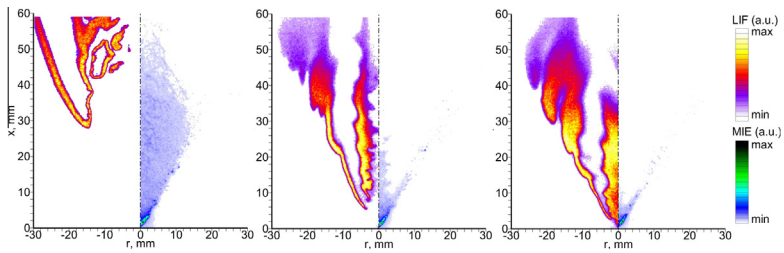

Fig. 5. Instantaneous OH PLIF and Mie scattering images for $D_{co} = 95$ mm and $\alpha = 60\%$ (type C), $\alpha = 40\%$ (type B) and $\alpha = 30\%$ (type A).

droplet cloud. This rapid vaporization of the homogeneous cloud of small droplets leads to mix rapidly the vapor produced and the oxygen in excess, leading to the partially premixed inner flame: the vapor and oxygen in excess burn in a lean premixed flame adjacent to a diffusion flame burning the excess of O_2 with fuel vapor cloud in periphery.

For the low values of α (type A), the inner flame is now anchored to the nozzle and shortened. The OH PLIF signal is very broad and fills the entire centerline region. The aspect of OH zone, with a signal behind the flame front, looks like that of a premixed flame. This oxyfuel flame with high concentration of O_2 produces high temperature burnt gases in the central part of the spray where small droplets are still present and can induce very short vaporization time (Table 2). Thus these small droplets vaporize very quickly in a gas very rich in oxygen. The inner flame is shortened ending where the vapor produced by the small droplets is consumed. At the outer boundary of the liquid sheet on the coflow side, the density and residence time of small droplets is not sufficient to allow a flame to establish.

The change in the combustion regime of the inner flame from diffusion-like (type C) to premixed-like (types A and B) shows the impact of the decrease in the vaporization time scale due to the presence of the flame. Table 2 illustrates that the vaporization time is divided by 100 when the flame is present. Thus, its presence close to the nozzle for types A and B leads to a rapid evaporation of the small droplets of the inner part of the spray merged in oxidant gas entrained to the spray axis, and then the rapid mixing of fuel vapor and oxidizer. The presence of the flame is controlled by the stabilization process, which depends on the α dilution ratio.

3.4. Flame stabilization

For the stabilization process as for the flame structure, the gas composition has to be distinguished from the total spray composition. The flame can stabilize where the gas composition is close to stoichiometry and the local gas velocity is suitable. In gas jet flames, the flame stabilizes where the flow velocity is of the order of S_L (between 0 and $3S_L$ [22]), what corresponds to the velocity of the upstream upcoming flow corresponding to $S_{TF} = \sqrt{\rho_u/\rho_b}\ S_L$ [23], due to streamline deflection.

In type C, the flame is lifted off and stabilizes in the downstream two-phase flow ($r = -10$ mm; $x = 20$ mm). The gas velocity has been measured very close to the flame base location ($r = -12$ mm; $x = 20$ mm): $U = -0.2 \pm 0.25$ m/s; $V = 0.8 \pm 0.17$ m/s, showing the strong deflection of the gas flow induced by the spray entrainment as illustrated in Fig. 3. These measurements show that the flame can meet the criteria $\bar{U}$ between 1 and $3S_L$, and is close to S_{TF} in average (Table 2). So far downstream ($h = 20$ mm), the droplets remain much faster than the gas: the big droplets ($D > 75$ μm) have kept high velocities (>15 m/s), the smallest droplets saw their velocity greatly reduced since their ejection from the liquid sheet, but their velocity keeps high. The size distribution just in front of the average flame base shows that the spray has vaporized at moderate temperature, with the fraction of the small droplets ($D < 25$ μm) greatly reduced providing a stoichiometric composition in this region, while the biggest droplets have little vaporized.

The type B is characterized by the stabilization of the double trailing flame at the tip of the liquid sheet where all the droplets are ejected at high velocity (above 20 m/s). Three phenomena lead to the flame stabilization just beyond the tip of the liquid sheet, while it must still meet the criteria of the gas composition and gas aerodynamics:

- The strong entrainment of the oxidant coflow, which deflects the outlying gas and brings a high quantity of coflow rich in O_2 towards the spray.
- The high oxyfuel flame adiabatic temperature, $T_F = 2693$ K (Table 2), leading to a very fast vaporization of the spray. This rapid vaporization of the whole spray leads also to a shift of the velocity distribution by size class (Fig. 6). Compared to cold condition deduced from data of C-flame (insert 95 mm, $\alpha = 60\%$), the same radial velocity distribution is found with a shift of 6 μm to the smaller diameter. The axial velocity has increased slightly by thermal expansion.

The decrease in α increases the burning velocity, SL, thereby enhancing the flame stabilization by facilitating the satisfaction of the criterion on the local gas velocity: $U = 0.67 \pm 0.23$ m/s;

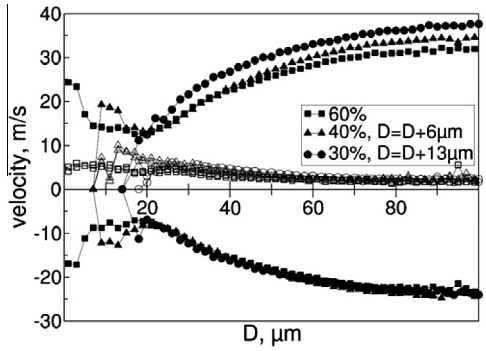

Fig. 6. Size-classified velocities at $r = -4$ mm, $x = 6$ mm, for three dilution α and $D_{co} = 95$ mm. Plain symbols for axial (top) and radial (bottom) mean velocities, open symbols for the corresponding fluctuations.

$V = 4.26 \pm 0.26$ m/s, while $S_L = 1.2$ m/s and $S_{TF} = 3.6$ m/s.

For the type A, the outer flame still stabilizes at the tip of the liquid sheet similarly to type B, with still increased values of T_F and S_L (Table 2). The vaporization is still faster than for type B due to increase in T_F and is confirmed in Fig. 6 by the shift of 13 μm of the velocity distribution compared to the cold case. As previously described, the rapid vaporization of the small droplets in the central part of the spray stabilizes the flame just beyond the nozzle exit.

4. Conclusion

The influence of CO_2 content on the structures and stabilization of spray oxyfuel flames has been investigated using a simplified configuration suitable for building database. The spray structure is characterized by size-classified analysis of its aerodynamics. Due to the polydispersion and the non-homogeneity in size and velocity, the flame exhibits a double structure specific to two-phase flames. This structure and the flame stabilization are strongly affected by the CO_2 content of the oxidant. The decrease in α leads to simultaneously shorten the vaporization and chemical time scales allowing the flame to stabilize just beyond the tip of the liquid sheet. The outer flame of the double structure is always diffusion-like while the inner flame changes from diffusion-like to premixed-like when the vaporization time shortens. All the results provide an original database suitable for numerical modeling as shown by the large-eddy simulation of N. Enjalbert [24].

Acknowledgements

This work was performed with the financial support of ADEME – France (Grant no. 0774C0038) and Air Liquide in the framework of the project SAFIR.

References

[1] M.B. Toftegaard, J. Brix, P.A. Jensen, P. Glarborg, A.D. Jensen, *Prog. Energy Combust. Sci.* 36 (2010) 581–625.
[2] D. Cieutat, I. Sanchez-Molinero, R. Tsiava, P. Recourt, N. Aimard, C. Prébendé, *Energy Procedia* 1 (2009) 519–526.
[3] H. Stadler, D. Christ, M. Habermehl, P. Heil, A. Kellermann, A. Ohliger, D. Toporov, R. Kneer, *Fuel* 90 (2011) 1604–1611.
[4] S. Hjärtstam, K. Andersson, F. Johnsson, B. Leckner, *Fuel* 88 (2009) 2216–2224.
[5] K. Andersson, R. Johansson, F. Johnsson, B. Leckner, *Energy Fuels* 22 (2008) 1535–1541.
[6] A. Amato, B. Hudak, P. D'Souza, P. D'Carlo, D. Noble, D. Scarborough, J. Seitzman, T. Lieuwen, *Proc. Combust. Inst.* 33 (2011) 3399–3405.
[7] P. Heil, D. Toporov, M. Förster, R. Kneer, *Proc. Comb. Inst.* 33 (2011) 3407–3413.
[8] D. Stepowski, A. Cessou, P. Goix, *Combust. Flame* 99 (1994) 516–522.
[9] A. Cessou, D. Stepowski, *Combust. Sci. Technol.* 118 (1996) 361–381.
[10] S.K. Marley, E.J. Welle, K.M. Lyons, W.L. Roberts, *Exp. Thermal Fluid Sci.* 29 (2004) 23–31.
[11] P. Domingo, L. Vervisch, J. Réveillon, *Combust. Flame* 140 (2005) 172–195.
[12] G. Continillo, W.A. Sirignano, *Combust. Flame* 81 (1990) 325–340.
[13] V.G. McDonnel, M. Adachi, G.S. Samuelsen, *Atomization Sprays* 3 (1993) 411–436.
[14] C. Maurey, A. Cessou, B. Lecordier, D. Stepowski, *Proc. Comb. Inst.* 28 (2000) 545–551.
[15] A. Cessou, C. Maurey, D. Stepowski, *Combust. Flame* 137 (2004) 458–477.
[16] G.T. Kalghatgi, *Combust. Sci. Technol.* 41 (1984) 17–29.
[17] A. Kourmatzis, W. O'Loughlin, A.R. Masri, *Flow Turbul. Combust.* 91 (2013) 405–427.
[18] COSILAB, The Combustion Simulation Laboratory, Version 3.1, Rotexo GmbH & Co. KG, Haan, Germany, 2007, <http://www.rotexo.com/cms/index.php>.
[19] N. Leplat, P. Dagaut, C. Togbé, J. Vandooren, *Combust. Flame* 158 (2011) 705–725.
[20] D.B. Spalding, *Proc. Combust. Inst.* 4 (1953) 847–864.
[21] P. Jenny, D. Roekaerts, N. Beishuizen, *Prog. Energy Combust. Sci.* 38 (2012) 846–887.
[22] L. Muñiz, M.G. Mungal, *Combust. Flame* 111 (1997) 16–31.
[23] G.R. Ruetsch, L. Vervisch, A. Liñan, *Phys. Fluids* 7 (7) (1995) 1447–1454.
[24] N. Enjalbert, Modélisation avancée de la combustion turbulente diphasique en régime de forte dilution par les gaz brûlés., Thèse de Doctorat (Nouveau Régime), INSA de Rouen, Rouen, 2011.